Phase diagram and phase transitions of monolayer and bilayer CF_4 on graphite

Q. M. Zhang, H. K. Kim,* and M. H. W. Chan
The Pennsylvania State University, Department of Physics, University Park, Pennsylvania 16802
(Received 28 April 1986)

The phase diagram of CF_4 adsorbed on graphite in the monolayer and bilayer region is mapped out in an ac heat-capacity study. In the monolayer region, the resultant phase diagram shows the existence of five different solid phases. The melting transition can proceed from the (2×2) commensurate, $I(S)$ (an incommensurate phase), and the hexagonal incommensurate (HI) phases. Strongly-first-order melting is found from the (2×2) and the $I(S)$ phases. In contrast, a sharp and small heat-capacity peak followed by a broad anomaly, similar to the melting of Ar on graphite in the submonolayer region, is observed at the melting of the HI phase. In the bilayer region, four different regions of coexisting solid phases are found. The melting of the bilayer solid occurs at a triple point at 89.05 K. Our data also suggest a bilayer critical point at 93 K.

I. INTRODUCTION

Due to the interplay of the substrate periodic field and the density variation of the adsorbed layer, the CF_4 on graphite system contains many different phases not observed in other adsorbate systems.[1-5] In the submonolayer region, scattering studies found three different solid phases: a three peak phase $3P$, an incommensurate phase $I(S)$, and a (2×2) commensurate phase. The $I(S)$ phase is thought in an earlier study to be a striped phase.[4] In addition, our heat-capacity data, to be reported below, suggest an additional incommensurate solid phase that exists between the $3P$ and the $I(S)$ phases. We shall label this the intermediate phase (IP). At the near-monolayer-completion coverages, melting transition proceeds from two different pure incommensurate solids as well as from the pure (2×2) commensurate phase. The richness of the monolayer phase diagram allows studies of various commensurate-incommensurate (C-I) transitions and melting transition from different solid phases. CF_4 on graphite is also special in that the commensurate phase is a (2×2) rather than the more common $(\sqrt{3}\times\sqrt{3})$ phase. The (2×2) phase is formed with the molecules located on the vertices of the graphite honeycomb.[1,4,5] As shown in Fig. 1, there are eight equivalent adsorption sites. The order-disorder transition of this (2×2) structure has been considered theoretically.[6,7] Depending on the detailed adsorbate-adsorbate and adsorbate-substrate interactions, this (melting) transition can be either first order or continuous.[6,7]

One challenging problem in the study of adsorption is to understand how these various monolayer phase evolve to bulk phases and how do the nature of the transitions between the phases change with increasing surface coverage.[8] A detailed study of the bilayer system is particularly important. In this coverage region, in addition to the usual competition between the vertical substrate-adsorbate interaction and the lateral adsorbate-adsorbate interaction, the interaction between adsorbates in different "layers" also plays a significant role. The CF_4 on graphite system, owing to its relatively low three-dimensional (3D) vapor pressure in the bilayer region, is suitable for the application of the high-resolution ac heat-capacity technique up to and beyond the melting temperature of the adsorbed layers.

Before discussing our results we shall first summarize previous experimental results of CF_4 on graphite. In the monolayer region, there are a number of inconsistencies among the various scattering results. In an early neutron scattering experiment,[1] five different solid phases were detected in the submonolayer region. Even if some of these may not be distinct phases, it is certain that at low temperatures the solid is in the so-called three peak phase ($3P$), where three diffraction peaks were seen. At 55 K a phase transition changes the solid to an incommensurate structure and at an even higher temperature, 65 K, a commensurate-incommensurate (C-I) transition is found. Above 65 K the solid film is in the (2×2) commensurate structure. A two-dimensional (2D) triple-point melting transition is found for this (2×2) phase at 75 K. According to a vapor pressure isotherm experiment by Dolle

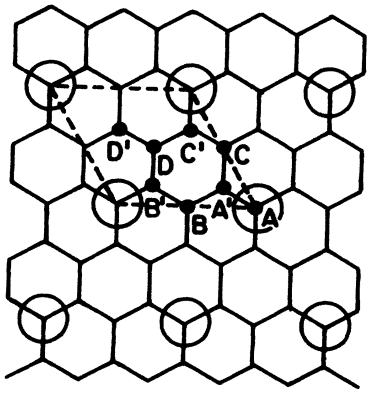

FIG. 1. $(2\times)$ commensurate phase of CF_4 on graphite. The honeycomb structure is the graphite substrate and the open circles denote the CF_4 molecules. A,B,C,D, and A',B',C',D', are eight equivalent adsorption sites within a unit cell.

et al.,[2] the liquid-vapor critical point is around 99 K. A low-energy electron diffraction (LEED) experiment was also performed on this system,[3] in the incommensurate phase between 55 and 59 K the overlayer was found to possess orientation order induced by the substrate. Due to the complication of many possible configurations, these scattering measurements were not able to determine the structures of the $3P$ and the incommensurate phases. Recently, two different synchrotron x-ray diffraction experiments were carried out. The first study (denoted as x-ray I) by Kjaer *et al.*[4] found evidence that the incommensurate phase detected in the earlier neutron study between $3P$ and (2×2) structures is likely a striped incommensurate (SI, as defined by Kjaer *et al.* in Ref. 4) or uniaxially compressed phase. In this phase the domain walls are parallel to each other and the adlayer is compressed anisotropically compared with the commensurate solid. Their result also indicated that a pure SI phase exists at higher coverages. At even higher coverages, the CF_4 layer is in a dense hexagonal incommensurate (*HI*) structure. The melting transition from the (2×2), SI, and *HI* phases were all interpreted as being continuous.[4] The results of a more recent synchrotron x-ray experiment[5] (denoted as x-ray II) differs from x-ray I in a number of important aspects. In particular, they dispute the existence of a SI phase. The authors interpreted their data, taken around 65 K, which is slightly below the *C-I* transition as indicative of a coexistence region of an incommensurate fluid with metastable patches of commensurate solid. At lower temperatures, the adlayer is in a uniformly compressed incommensurate solid phase. This situation looks similar to that of the *C-I* transition of Kr adsorbed on graphite where a fluidlike region intervenes the commensurate and incommensurate solid phases.[9]

The structures of the bilayer solid phases are unclear at this point. By extrapolating the high-temperature vapor pressure isotherm data, Dolle *et al.*[2] suggested that CF_4 does not wet graphite at low temperatures and at 65 K there is a single layer-bilayer layering transition. They also found a bilayer critical point at 106 K. The early neutron scattering study[1] on the bilayer region seemed to be consistent with the isotherm observation that CF_4 at low temperatures forms a single layer on graphite that coexists with bulk clusters.

Results of an ac heat-capacity study[10,11] on CF_4 on graphite is reported here. The resolution of our heat-capacity determination is 0.2% and the absolute value of the heat capacity can be determined to within 10%. In this study, a total of 45 heat-capacity scans were made. In each scan, a heat-capacity measurement was carried out as a function of temperature for a fixed amount of CF_4 in the sample cell and the experiment ranges from 18 to 106 K. Since a fixed coverage heat-capacity scan is not sensitive in detecting phase boundaries that are parallel to the temperature axis, vapor pressure isotherms at 75, 96, and 100 K were made to complement the heat-capacity study.

The organization of the remainder of this paper is as follows. In Sec. II the phase diagram of CF_4 on graphite based on this study is presented; in Sec. III transitions in the submonolayer region are discussed; in Sec. IV we describe the melting in the (2×2) phase; in Sec. V the melting in $I(S)$, and *HI* phases; in Sec. VI the phase diagram in the bilayer region is reported. A summary is presented in Sec. VI.

II. PHASE DIAGRAM

The proposed phase diagram is shown in Fig. 2. The notations for each phase in the phase diagram are consistent with that used by other studies. Since the existence of a striped phase is controversial, we used symbol $I(S)$ to denote this incommensurate phase. In our phase diagram, an $n=1$ coverage is defined as a (2×2) completed layer. This coverage scale was determined by a nitrogen isotherm at 74 K.[10] This isotherm as well as an isotherm performed at 96 K with CF_4 are shown in Fig. 3. In the ideal case, the number of particles required to form a (2×2) monolayer is $\frac{3}{4}$ of that necessary to form a $(\sqrt{3}\times\sqrt{3})$ monolayer. Therefore the coverage for a (2×2) overlayer inferred from the end point of the liquid-solid coexistence region of the 74-K N_2 isotherm is 9.94×10^{18}. Due to the very low vapor pressure value, the phase boundary between the $I(S)$ phase and the fluid phase cannot be resolved in the CF_4 isotherm. Since the population of vacancies in the CF_4 (2×2) and the N_2

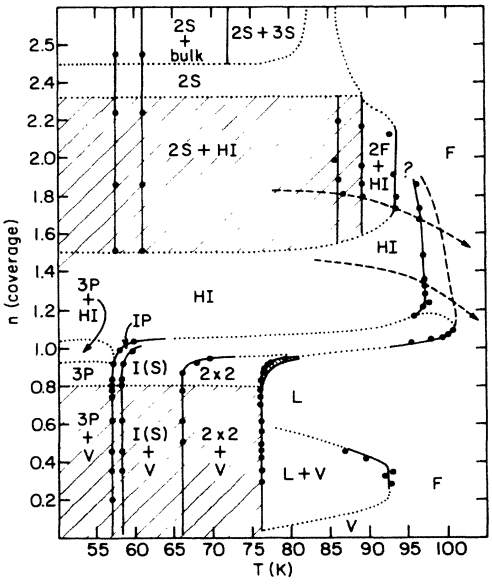

FIG. 2. Proposed phase diagram based on this study. Solid circles are location of observed heat-capacity anomalies. Solid lines are proposed phase boundaries. Dotted lines are more speculative phase boundaries. Dashed lines with arrow indicate real experiment paths after desorption correction. A dashed line separating the well-correlated fluid from the isotropic fluid is also shown. In the submonolayer region, the triple-point melting ends near $n=0.6$. Hatched region in the monolayer denotes the solid-vapor coexistence. Above $n=0.7$, the melting signal broadens but still stays at the triple point temperature up to approximately $n=0.8$. A narrow coexistence region of (2×2) and liquid is found along the (2×2) and L boundary. In the bilayer region, there are four different solid phases coexisting with the first layer *HI* phase, also shown as a hatched region. The first layer *HI* phase melting line may terminate in the bilayer region near 93 K and $n=2.0$.

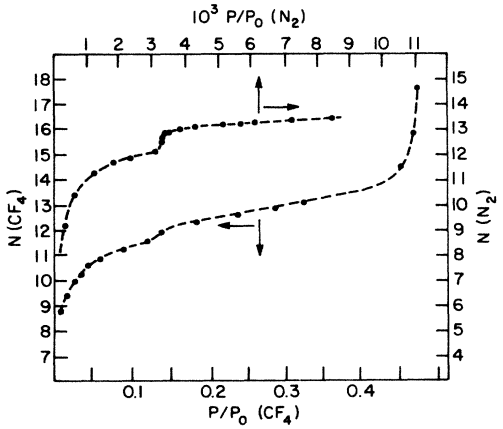

FIG. 3. Vapor-pressure isotherm for N_2 at 74 K (top curve) and CF_4 at 96 K (bottom curve). The substep in the N_2 isotherm is the solid-fluid coexistence region and the end point of that region is used to define a complete $(\sqrt{3}\times\sqrt{3})$ monolayer. The kink in the CF_4 isotherm near $n\sim 11.8\times 10^{18}$ is the phase boundary between the $I(S)$ phase and the HI phase. The number of adsorbate is in units of 10^{18} molecules for both N_2 and CF_4.

$(\sqrt{3}\times\sqrt{3})$ structures and the stability of those phases against the formation of other incommensurate phases may be different, the (2×2) completion coverage inferred from the N_2 isotherm may be, and is found to be, different from the actual coverage for the completion of a (2×2) CF_4 monolayer on graphite. We will return to this point later.

The overall structure of our phase diagram in the monolayer region is similar to that based on scattering experiments but the temperature of some phase boundaries are substantially different. Our coverages for the completion of (2×2) layer and for the boundary separating the $I(S)$ and HI phases near 85 K are in much better agreement with the x-ray-I study. In the x-ray-I study, the ideal (2×2) completion coverage ($n=1$) is defined against the upper boundary of the Kr on graphite $(\sqrt{3}\times\sqrt{3})$ solid. In our coverage scale, $n=1$ is defined against the lower boundary of the pure $(\sqrt{3}\times\sqrt{3})$ phase of N_2.[10] In order to match the two coverage scales, a reduction by a factor of 1.1 should be applied to our coverage scale. If this normalization factor is applied, the phase boundary between the $I(S)$ and HI phase below 90 K in our phase diagram is found at $n=0.94$, in good agreement with the x-ray-I result.

The new features from our phase diagram are as follows. In the submonolayer region, a new intermediate phase labeled as IP phase, is proposed between the $3P$ and $I(S)$ phases over a narrow temperature range of about 1 K. The IP phase may also extend to higher temperatures sandwiching between the HI and $I(S)$ phases. In the region near monolayer completion, our phase diagram shows the melting of CF_4 on graphite can proceed from the (2×2), $I(S)$, and HI phases. The melting transitions of the (2×2) and $I(S)$ phases are strongly first-order processes. The melting transition of the HI phase occurs at a lower temperature and shows features similar to that observed for the melting of submonolayer Ar on graphite.[12] This suggests that the melting transition is a weakly first-order, two-step process.[13] Above monolayer completion region four different coexisting solid regions are found. The melting of the bilayer solid occurs at 89.05 K, the bilayer triple point. The critical point of the bilayer is found near 93 K.

III. TRANSITIONS IN THE $n<1$ REGION

In the submonolayer region, with coverages less than $n=0.8$, the solid phases coexist with 2D vapor. In our phase diagram we propose that there are four different solid structures. With increasing temperature we find the $3P$ phase, the intermediate phase IP, the $I(S)$, and the (2×2) phase.

Between 18 and 50 K we found no heat-capacity anomaly within our resolution (0.5 k_B per molecule). At 57.15 K a prominent heat-capacity peak was found. Comparing our result with that from x-ray and other scattering stud-

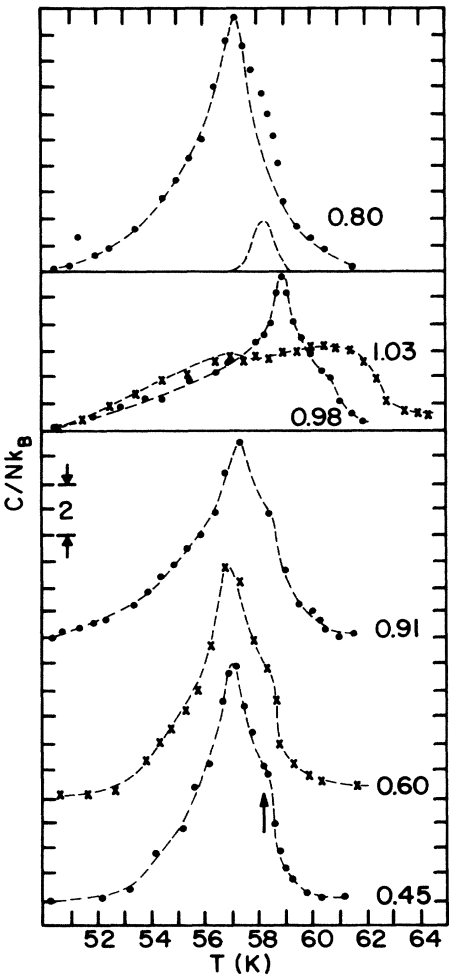

FIG. 4. Heat-capacity signals near 57 K at different coverages. Notice the small side peak around 58.4 K. In the top panel, the side peak and the main peak are separated as two distinct Gaussian-like peaks. In the middle panel, the $n=0.98$ and 1.03 scans are shown together to show the low-temperature tail indicating the existence of phase boundaries near these coverages.

ies,[1,4] we identify this peak to be related to the transition from the $3P$ phase. The heat-capacity traces for this signal are presented in Fig. 4. The data is shown with the background from the calorimeter and the regular part of the heat capacity of the overlayer subtracted. From Fig. 4 it can be seen that this prominent peak stays at 57.15 K in the entire submonolayer region. Beyond $n=0.8$, the peak positive moves gradually towards higher temperatures. At $n=1.03$, this peak broadens significantly, indicating that the phase boundary represented by this signal becomes nearly parallel to the temperature axis. At a slightly higher coverage ($n=1.07$) no heat-capacity anomaly around this temperature is detected. The characteristics of this transition signal are summarized in Table I.

There are two points we wish to make about this 57.15-K signal. Firstly, the shape of the peak indicates the possibility of two phase boundaries separated by about 1.2 K. Secondly, there is a large entropy change involved in this transition. The first observation is based on the fact that in addition to the main peak at 57.15 K there is a side peak near 58.4 K. The significant difference in the peak sizes between the main peak at 57.15 K and the side peak at 58.4 K as shown in Fig. 4 indicates the different nature for the two heat-capacity anomalies. The presence of the vapor phase in the submonolayer region rules out the interpretation of a three phase (two solid phases in addition to vapor) coexistence region between 57.15 and 58.4 K. Instead, we propose a new phase in this 1.2-K temperature region. We have tentatively identified this to be the intermediate or IP phase.

We have calculated the total area under this signal. As we show in Fig. 5 the transition entropy change for this entire heat-capacity anomaly is comparable to or even greater than that of the (2×2) melting at the triple point. In bulk CF_4, there is a solid-solid transition, called the α-β transition, at 76.2 K.[14] This is an orientational ordering transition with concomitant structural changes. The α-β transition also has a much larger transition heat than the bulk triple-point melting.[14] In the 2D system, the anisotropic coupling between CF_4 molecules may produce an orientationally ordered phase at low temperature that undergoes a transition to a disordered phase as temperature is increased. The transition temperature and the large transition heat involved in the 57.15-K main peak suggest that this is an orientational ordering transition. The so-called $3P$ phase that resists structural determination from the scattering studies may be due to a complicated coupling of the orientational and translational degrees of freedom (large unit cell or domain structure due to the molecular orientations). The nature of the IP phase in the small temperature interval is unclear and further scattering study is required.

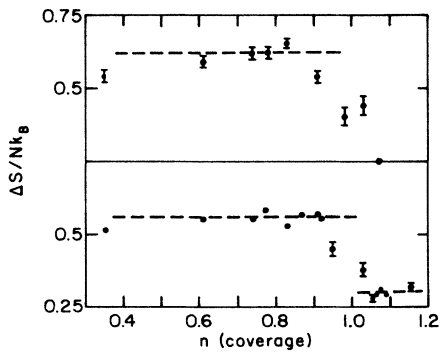

FIG. 5. Integrated area under the heat-capacity peak for the 57 K anomaly (top panel) and the melting transition (bottom panel) as a function of coverage. Top panel indicates a phase boundary just below $n=1.07$. Bottom panel indicates melting transitions for $n<0.9$ and $n>1.0$ are from different solid phases.

TABLE I. Heat-capacity features for the 57.15-K peak. FWHM is the full width at half maximum. Two separate runs were made using two different cells, the data of $n=0.35$, 0.775, and 0.80 are taken from the second run.

Coverage (n)	Peak position (K)	Peak height (C/Nk_B)	FWHM (K)
0.20	57.15	8.5	2.2
0.35	57.10	10.5	2.2
0.45	57.15	9.0	2.6
0.60	57.10	8.5	2.7
0.61	57.10	8.6	2.9
0.74	57.15	8.5	2.9
0.775	57.20	10.0	2.8
0.78	57.15	8.0	3.15
0.80	57.40	9.60	2.7
0.83	57.30	8.0	3.3
0.91	57.40	7.6	2.95
0.98	58.15	6.0	2.25
1.03	A broad peak exists between 60 and 62 K.		

As coverage goes above $n=0.8$, the adlayer is in a pure solid phase. In the pure solid phase both the 57.15-K heat-capacity anomaly and the side peak shifts to higher temperatures with increasing coverage. Figure 4 shows that the heat-capacity scans at $n=0.98$ and 1.03 in this temperature range are different from that at lower coverages. A long tail appears on the low-temperature side of the peak at $n=0.98$. This low-temperature feature becomes more prominent for the $n=1.03$ scan. The transition entropy under the whole signal also diminishes with coverage. The main peak for the $n=0.98$ scan is significantly sharper than those at lower coverages. It is possible that in the so-called $3P$ phase, as suggested by the neutron study,[1] there is significant density variation in the overlayer. This interpretation would suggest the anomalies observed in scans with n less than 0.98 are from the $3P$ phase and that at $n=0.98$ from the HI phase. For scans at coverages higher than $n=1.03$, no heat-capacity anomaly is seen in this temperature range. A reasonable interpretation is that a phase boundary almost parallel to temperature axis lies near $n=1.03$. The tentative phase diagram, including the more speculative boundaries shown as dotted lines in Fig. 2 in this region is consistent with these considerations. The $3P+HI$ coexistence region above the pure $3P$ phase is consistent with the x-ray-I result.[4]

The C-I transition between the $I(S)$ and (2×2) structures has a very small heat-capacity signal as shown in Fig. 6. The transition temperature in the submonolayer region is near 66.4 K. The peak height is only about 1 k_B per molecule. Scattering experiments[1,4,5] indicate that the change of the lattice constant of the adlayer at this transition is continuous, our result is consistent with this observation. As mentioned in the Introduction, the x-ray-II experiment[5] suggests the existence of an incommensurate fluid phase between the (2×2) and the incommensurate solid [our $I(S)$] phase. We do not find two heat-capacity signatures corresponding to entering and leaving this fluid phase. It is possible that the transition signal is too weak to be detected for one of these two boundaries or there is no distinct phase boundary between the so-called incommensurate fluid and the solid phase.

The phase boundary of this C-I transition moves to higher temperature for coverages higher than $n=0.9$. The boundary separating the commensurate (2×2) and the $I(S)$ phase near $n=0.95$ appears to be parallel to the temperature axis. Compared with the C-I transition boundary of the N_2 $(\sqrt{3}\times\sqrt{3})$ phase at $n=1.1$ (Ref. 10), the C-I boundary between the (2×2) and $I(S)$ phases at $n=0.95$ for CF_4 is remarkably low. One interpretation is that the (2×2) phase contains a great deal of vacancies and this commensurate phase is not stable against the formation of an incommensurate overlayer with increasing 2D spreading pressure. This (2×2) phase is also not stable against changes in temperature, as exhibited in the triple point, rather than incipient-triple-points-like melting of commensurate Kr, N_2 overlayers.[15] We will discuss this in more detail in the following.

At 76.3 K a δ-function-like heat-capacity anomaly was observed in the submonolayer region. By comparison with scattering results we were able to identify this as the melting transition of the (2×2) solid at a triple point. The liquid-vapor critical point is near 93 K according to our measurement. The heat-capacity traces for these signals are shown in Fig. 7. The melting signal is sharp with a reduced peak height C/Nk_B of 100 and a half width of 0.25 K. The transition heat is about $42k_B$ K. For bulk CF_4, this value is $84k_B$ K at the triple point temperature of 89.5 K.[14]

The triple-point melting of CF_4 on graphite is unusual in that the solid patches are commensurate with the substrate. In other adsorption systems, triple-point melting is found only from incommensurate solids. For $(\sqrt{3}\times\sqrt{3})$ commensurate solid of classical adsorbates such as N_2 and Kr,[15] the melting transition at submonolayer goes through a so-called incipient triple point. There is no liquid-vapor coexistence region and no critical point in the phase diagram of N_2 and Kr on graphite. The physical origin of the incipient triple-point melting is that the substrate adsorption barrier lowers the energy of the commensurate solid in comparison with the liquid phase. This effect causes the solid to melt at a higher than "normal" melting temperature.[15,16] If this melting occurs above the "expected" liquid-vapor critical temperature, melting proceeds from solid-fluid coexistence directly into a homogeneous fluid phase.

The ratio $T_t(2D)/T_t(3D)$ is usually used to measure the stability of the two-dimensional solid, where $T_t(2D)$ and $T_t(3D)$ are, respectively, the melting temperatures of the two-dimensional solid and bulk. For CF_4 on graphite, this number is 0.85. Compared with other systems this value is extremely high, even higher than systems that melt from commensurate solids such as Kr (0.73) and N_2 (0.78).[17] It would be misleading to conclude that CF_4 should have a melting behavior like that of N_2 and Kr on graphite. We think $T_t(3D)$ is not a good quantity to use since the bulk triple-point temperature depends on com-

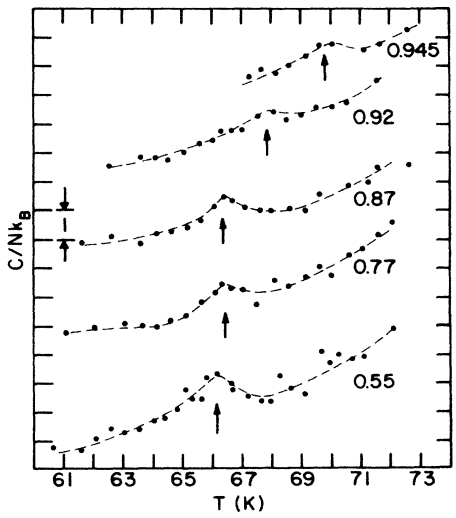

FIG. 6. Heat-capacity anomaly for the (2×2) to $I(S)$ C-I transition. The peak positions are indicated by arrows.

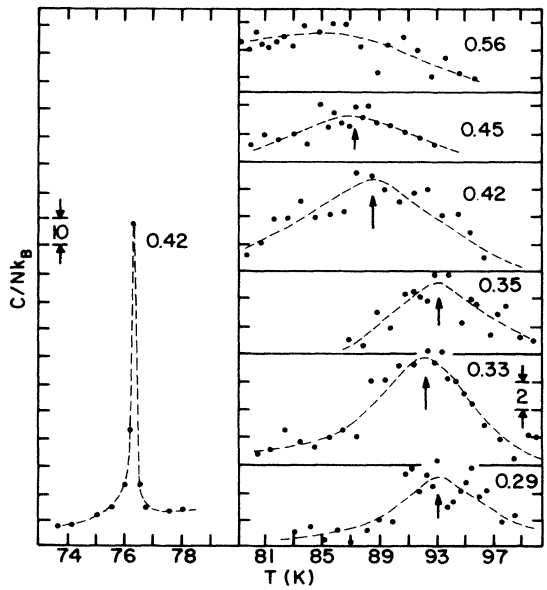

FIG. 7. Heat-capacity traces for the melting and the liquid-vapor transitions in submonolayer coverages. Different scales in the heat capacity and temperature are used for the melting and the liquid-vapor signals. Dashed lines are drawn to guide the eye and the arrows indicate the positions of the peak.

plicated factors such as the symmetry and coordination number of the solid. It is more suitable to compare $T_t(2D)/T_c(3D)$ of the various system because $T_c(3D)$, the bulk critical temperature, is not dependent on the structure of the 3D solid. For CF_4, this number is 0.33, which is comparable to other incommensurate solids on graphite, while for N_2 and Kr this value is about 0.39. This suggests the corrugation of the graphite substrate for the CF_4 (2×2) overlayer, unlike that for Kr and N_2 $(\sqrt{3}\times\sqrt{3})$ overlayer, is not sufficient to stabilize the CF_4 (2×2) phase beyond the "normal" melting temperature. A recent model calculation also found triple-point melting from the commensurate solid when the substrate corrugation is not sufficiently strong.[16] The weak corrugation of the substrate for the CF_4 (2×2) phase is mainly due to the fact that the adsorption sites are on the vertices rather than the centers of the graphite honeycomb.

In addition to the melting signal, heat-capacity anomaly related to crossing the liquid-vapor boundary is found at a higher temperature for coverages between $n=0.29$ and $n=0.59$. The critical point temperature is at 93 ± 1 K, which is lower than the value obtained from the isotherm data at 99 K.[2] It is clear that in detecting such a phase boundary which is nearly parallel to the coverage axis, the fixed coverage heat-capacity measurement is superior to the vapor pressure isotherm technique. In the isotherm studies, the critical temperature is determined by extrapolating the compressibility as a function of temperature from isotherm data obtained at $T>T_c$. Such a linear extrapolation procedure tends to give a T_c higher than the correct value since the critical exponent γ characterizing the compressibility in a 2D liquid-vapor transition is 1.75 rather than 1.[18,19]

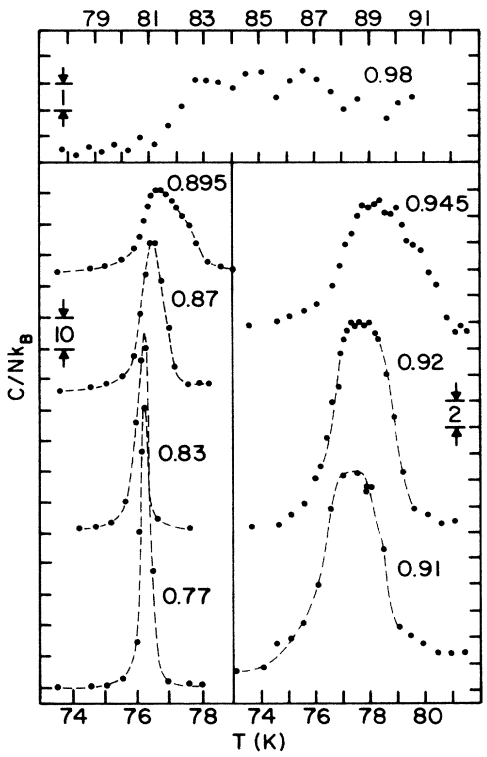

FIG. 8. The melting signals for the pure (2×2) solid. Different scales are used in the different portion of the figure.

IV. MELTING TRANSITION IN THE (2×2) COMMENSURATE SOLID PHASE

In the following two sections we are going to present data on the melting transitions of the (2×2), $I(S)$, and HI structures. A summary of these results is contained in a short communication.[13] Shown in Fig. 8 is the melting signal from the pure (2×2) phase. This pure solid phase spans a coverage ranging from approximately $n=0.8$ to 0.95. It has been proposed that the order-disorder transition (melting) of this structure belongs to Heisenberg-type transition with "corner type" anisotropy and the eight equivalent ground states correspond to the eight corner directions in a cubic magnet. The order of the transition depends on the detailed interactions within the system.[7] The melting peak for the scan at $n=0.775$ is essentially at the submonolayer triple-point temperature. The half width of the peak [full width at half maximum (FWHM)] at 0.4 K is larger than that from scans taken at lower coverages ($n\leq0.6$) at 0.25 K due to triple-point melting. The scan at $n=0.87$ shows more clearly the broadening of the signal as well as a shift in the melting temperature. In addition, the peak shape becomes asymmetric indicating in addition to the main peak at 76.6 K there is another anomaly situated on the high temperature side of the main peak. For $n=0.895$, this side peak is at 77.3 K. Upon a slight increase from $n=0.895$, this side peak grows significantly. The melting signals for $n=0.91$ and $n=0.92$, as shown in Fig. 8 contain flat top in the peak region. These characteristics are not consistent with the interpretation of a continuous transition with finite-size rounding effect. We interpret this peak to be a signature of a first-order transition with narrow coexistence region of the (2×2) solid and liquid phases. The strong melting anomaly observed in the triple-point region and the large density discontinuity at melting near the triple point as shown in Fig. 2 are both evidences of a large density change between the solid and liquid phases. These are consistent with the presence of solid-liquid coexistence region for the melting of the pure (2×2) phase. No evidence of crossing over from first order to continuous-like behavior is found over the entire (2×2) coverage.

At $n=0.945$, the heat-capacity peak shows a great deal of fluctuations and the peak broadens significantly. The fluctuation is probably due to being very close to a flat phase boundary parallel to the temperature axis. This is the phase boundary separating the (2×2) and the $I(S)$ phases. As we will see below, although the experimental path of the $n=0.103$, 0.98, and 0.945 scans crosses the phase boundaries at similar angles, these heat-capacity scans are distinctly different. The $n=0.98$ scan shows more fluctuations over a large temperature range from 82 to 91 K. Although the detailed phase boundaries in this region are not clear, our data indicates that the phase boundary separating the (2×2) and $I(S)$ incommensurate phases lies between $n=0.95$ and 0.98. A recent heat-

TABLE II. The melting transition signal in the (2×2) phase.

Coverage (n)	Peak position (K)	Peak Height (C/Nk_B)	FWHM (K)
0.29	76.50	90.0	0.25
0.35	76.45	140.0	0.20
0.42	76.25	110.0	0.25
0.45	76.30	125.0	0.25
0.48	76.30	110.0	0.25
0.56	76.25	120.0	0.25
0.61	76.30	114.0	0.25
0.70	76.10	93.0	0.40
0.74	76.10	75.0	0.45
0.775	76.30	90.0	0.40
0.83	76.15	69.0	0.40
0.87	76.55	48.0	0.83
0.895	76.70	25.8	1.58
0.91	77.30	14.4	2.33
0.92	77.60	15.4	2.40
0.945	79.30	9.5	3.20
0.98	85.00	~3	~5

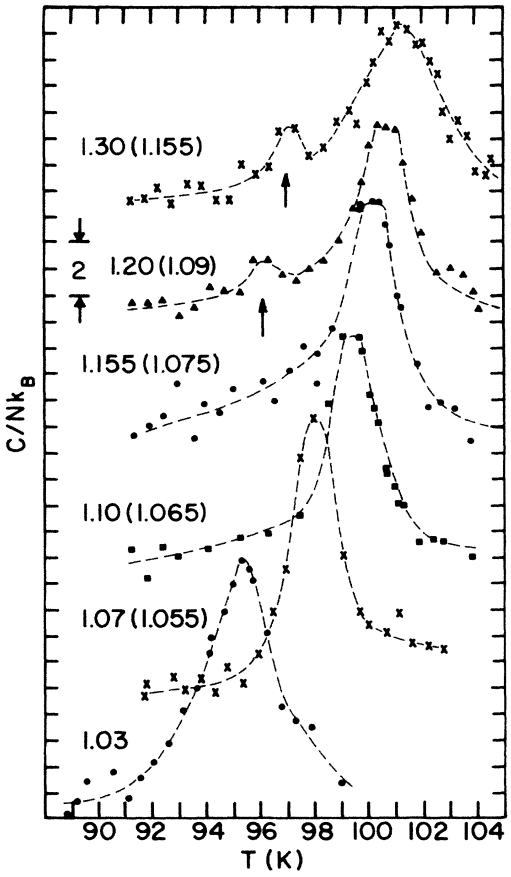

FIG. 9. Heat-capacity anomalies for the melting of $I(S)$ solid. The heat capacity is expressed in reduced unit, C/Nk_B, where N is the number of CF_4 molecules at low temperature with no desorption correction. The prominent heat-capacity peak is the melting for the $I(S)$ phase. The coverage shown in parentheses includes desorption correction at the melting point. There is a small side peak at lower temperature for the two high coverage scans. This peak is related to the melting of the *HI* phase, see Fig. 11 and Table III.

capacity study of N_2 on graphite found a narrow coverage region of coexisting commensurate and incommensurate solid phases at low temperatures.[10] Recent synchrotron x-ray experiments of Kr on graphite[9] at the high-temperature region found evidence for a fluidlike phase that exists between the commensurate and incommensurate solids.[20] A similar fluidlike phase between the (2×2) and $I(S)$ phases was suggested by x-ray-II study.[5] We are not able to draw firm conclusions regarding this possibility; phase diagrams with different boundaries can be drawn to connect the *C-I* transition region to the melting regions of the (2×2) and $I(S)$ phases.[21]

The heat of melting for this pure (2×2) phase is shown in Fig. 5. It has the same value as that at the triple point in the submonolayer region. Near $n=0.95$, this quantity begins to decrease and stays at a smaller value for $n>1.05$. This signifies a change in the solid overlayer from the (2×2) phase to the $I(S)$ phase. Our conclusion of a first-order melting for the (2×2) phase is consistent with the x-ray-II result.[5] The characteristics of the melting peak from submonolayer to $n=0.98$ are shown in Table II.

V. MELTING TRANSITIONS IN THE $I(S)$ AND *HI* PHASES

With a slight increase in coverage above $n=0.95$, the melting transition shifts rapidly to higher temperature as shown in Fig. 2. From the discussion above about the *C-I* transition boundary, and with reference to the scattering results, we identify the melting transition here as the melting from the incommensurate $I(S)$ phase. The heat-capacity scans in this coverage region are presented in Fig. 9. Since the 3D vapor pressure in this coverage-temperature region is substantial, desorption of CF_4 molecules from the graphite surface causes a temperature-dependent effective surface coverage. A symbol of n_e is used to denote this effective coverage. In Fig. 9, the heat capacity is expressed in the reduced unit of C/Nk_B, where N is the amount of CF_4 at low temperatures without desorption. The real reduced value of the heat capacity at each transition temperature ought to be rescaled by the effective coverage at that temperature. Except for Fig. 9 and later on for Fig. 10, the rescaled values are used in the subsequent discussion. It should also be noted that desorption affect may also alter the value of the measured heat capacity directly. This effect, however, is not expected to be significant. This is the case since the difference in the isosteric heat of adsorption in two different phases (e.g., solid and liquid) is on the order of the heat of transition, and Δn_e is much smaller than n_e throughout the transition region. The shape of the heat-capacity anomaly at $n=1.03$ is different from that at $n=0.945$ and 0.98 as mentioned in the preceding section.

This confirms our interpretation that the nature of the solid overlayer in these two regions are different and that a phase boundary parallel to the temperature axis exists near $n=0.95$. At higher coverages, the melting signal is a strong anomaly with a flat central region, similar to that observed for (2×2) melting. The transition entropy for this peak as shown in Fig. 5 is about half of that for the (2×2) phase. Following the same argument used in the melting of (2×2) phase, the melting transition in this region is interpreted as first-order-like and the heat-capacity peak signals the crossing of a coexisting solid-liquid region.

As pointed out in the Introduction, the nature of this incommensurate $I(S)$ phase is still controversial. If it is a striped incommensurate phase, the melting process, according to a model calculation, should be a two step process.[6] Because of the anisotropic property of the striped incommensurate phase, melting does not bring the system directly into an isotropic liquid phase; instead, there is an anisotropic fluid phase with (2×1) symmetry intervening between the striped and liquid phases. The melting from the striped to this (2×1) fluid phase is expected to be Kosterlitz-Thouless-like (KT).[6] Since the appearance of the flat central region in the observed heat-capacity anomalies can be interpreted as being due to two unresolved peaks, it might be tempting to argue that the heat-capacity anomaly is consistent with the two step melting process rather than our interpretation of a first-order melting with a coexistence region. This is unlikely to be correct. We have decomposed the heat-capacity anomaly into two symmetric subpeaks and found that each of the resultant peaks is more consistent with a first-order transition interpretation rather than continuous. Indeed, in a KT-like melting, no sharp heat-capacity peak is expected at the melting temperature.[22] A first-order-like peak is not expected for the melting from the (2×1) fluid to an isotropic liquid either, since this transition should be second order. Therefore either the $I(S)$ phase is not a striped phase, or the melting from the striped phase is a first-order process.

The melting transition from the *HI* phase, the most dense solid phase in the monolayer phase diagram is quite different from that of the (2×2) or the $I(S)$ phase. The heat-capacity scans for this coverage range are shown in Figs. 9 and 10. These heat-capacity scans suggest a change in the melting behavior between $n=1.20$ and 1.34. The $n=1.20$ scan shows a small side peak near 96 K in addition to the large flat-topped anomaly near 100 K characteristic of the $I(S)$ melting observed at lower coverages. An isotherm taken at 96 K also shows a kink signifying a phase transition in this coverage region (Fig. 3). As surface coverage is increased from $n=1.20$ to 1.40, the small side peak sharpens and moves to 97 K. Concomitant with this, the large peak near 100 K broadens significantly (the FWHM increases by a factor of 2) and loses its flat central region.

The heat-capacity scans shown in Fig. 10 are similar to that observed for the melting of Ar on graphite in the submonolayer region.[12] For Ar on graphite, a small ($3k_B$ per molecule) but sharp (FWHM of 0.3 K) peak near 47.2 K followed by a broad anomaly near 49 K was observed.

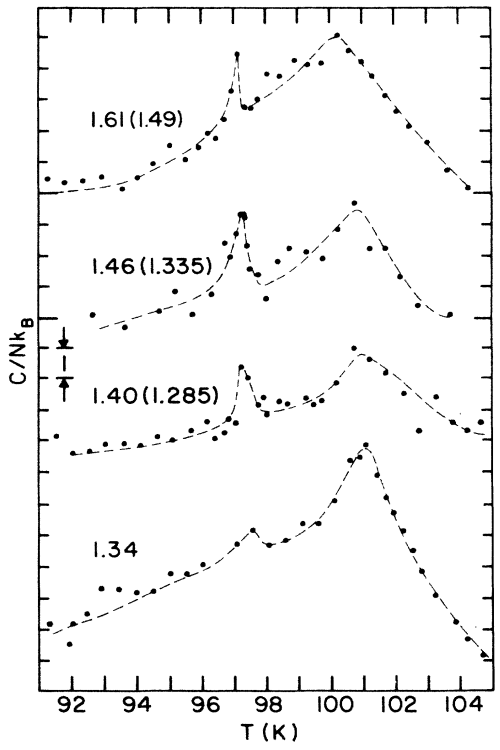

FIG. 10. Heat-capacity traces for the melting transition of *HI* solid. Heat capacity is expressed in the reduced unit C/Nk_B, where N is the number of CF_4 molecules on the graphite surface with no desorption correction. The sharp and small peak is the position of the *HI* phase melting. The coverages shown are that at low temperature, the desorption corrected coverages at the melting point are shown in parentheses.

The small sharp peak was interpreted to be due to a sudden, 0.2%, decrease in the density of the overlayer at melting. For CF_4 in the *HI* phase, the sharp peak near 97 K has a half width of about 0.4 K and a peak height of $2.1k_B$ at $n=1.40$. This heat-capacity peak corresponds to an entropy change, $\Delta S/Nk_B$, of about 0.01, which is comparable to the Ar case.[12] The entropy change of the broad heat-capacity peak near 101 K, $\Delta S/Nk_B$, is about 0.15. The relative position, T_s/T_b, of the small, sharp peak at T_s and the broad high-temperature peak at T_b for CF_4 is also comparable to that for Ar. It is about 0.96 for CF_4 and 0.95 for Ar. The size of this small heat-capacity anomaly increases for scans at $n=1.46$ and 1.51 by about 40%, then decreases until barely visible at $n=2$. Beyond $n=2$ this small peak is buried in the scatters in the data.

Since the changes in entropy from a solid to an isotropic fluid phase should be comparable for the $I(S)$ and *HI* phases, it is reasonable to consider both the sharp and the broad high-temperature peaks observed in the scans for the *HI* phase to be related to the melting transition. The melting from the *HI* phase is therefore a two step process; the first step is weakly first order at 97 K, and the second is likely to be continuous. The small change in entropy

that is related to the sharp peak at 97 K for the *HI* phase suggests that the intermediate phase just about 97 K is in a well correlated state, e.g., an orientationally ordered fluid phase. The broad peaks near 101 K corresponds to the transition from this well correlated fluid phase to an isotropic fluid phase. It is unclear to us whether the intermediate well-correlated fluid phase is a hexatic phase as proposed by the Kosterlitz-Thouless-Nelson-Halperin-Young (KTHNY) melting theory[22] or that the correlation in this phase is mainly generated by the coupling to the substrate's periodic corrugation.[12] Further careful scattering studies may be helpful to settle this issue.

The weakly first-order, two step melting observed in both Ar and CF_4 on graphite in different coverage range is striking. Recent computer simulation of Saito[23] and the model calculation of Chiu[24] found that the dislocation core energy is crucial in determining the order of the melting transition. The transition can change from a strongly first order to a weakly first order as the core energy increases. We do not know if the observed weakly first-order, two step melting in Ar and CF_4 systems can be fitted into this picture.

A detailed phase diagram in this region for the melting of the $I(S)$ and *HI* phases is shown in Fig. 11. The melting temperature for the *HI* phase is defined at the position of the small and sharp heat-capacity anomaly. Our phase diagram implies a tricritical point near $n_e = 1.13$ and the melting between the $I(S)$ and the well-correlated fluid is continuous. This is speculative, since the transition may in fact be weakly first order and a narrow $I(S)$ and well-correlated fluid coexistence region may extend to temperature well below 100 K. This coexistence region being almost parallel to the temperature axis, is difficult to detect with our technique. In Table III, we listed the melting features of the *HI* phase and $I(S)$ phase, the desorption corrected coverages at each peak temperature are also presented in Table III.

Since the boundary separating the (2×2) and $I(S)$ phases and that separating the $I(S)$ and *HI* phases as shown in Figs. 2 and 11 are parallel to the experimental path, the nature of these two solid-solid transitions and how these boundaries are connected to the melting lines of the (2×2), $I(S)$ and *HI* phases cannot be determined in this study. In the following, we propose speculative, but simple, possibilities based on what we have learned in other systems.[9]

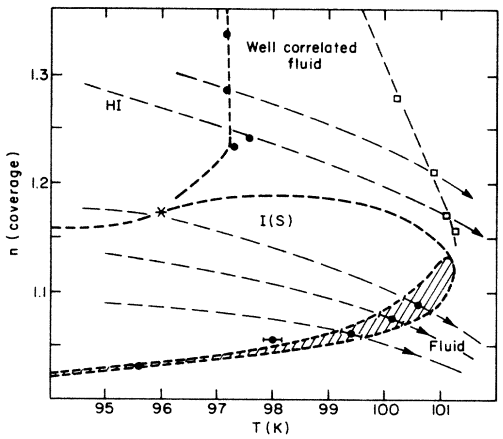

FIG. 11. Phase diagram in the vicinity of the melting transition of the $I(S)$ and *HI* phases. The coexistence region of $I(S)$ and liquid is shown to terminate near $n_e \sim 1.13$ and 101 K. This region may persist to low temperature along the boundary separating $I(S)$ and well-correlated fluid phases. The open squares denote the position of the center of the broad heat-capacity anomaly in the *HI* phase melting. The asterisk indicates the position taken from the kink of the 96 K isotherm and the heat-capacity peak at $n = 1.20$ scan. The real experimental paths are indicated by dashed lines with arrow. For details, see text.

(1) A reentrant fluid,[5,9,20] similar to that observed in Kr on graphite, exists between the (2×2) and the $I(S)$ phases. The transitions from the (2×2) to the reentrant fluid phase and from the reentrant fluid to the $I(S)$ phase are both continuous. There exist tricritical points in both the $I(S)$ and (2×2) melting lines separating first order and reentrant continuous melting.

(2) As shown in Fig. 11, the well-correlated fluid phase may extend to low temperature as a thin sliver separating

TABLE III. The melting signals above the (2×2) phase. In the table, a blank space means this quantity does not exist or is unclear; the asterisk means the quantity is hard to get. For each peak the four numbers represent the effective coverage n_e, peak temperature (in K), peak height (in C/Nk_B), reduced unit), and FWHM (in K).

Coverage (n)	Low-temperature peak	High-temperature peak
1.03		1.03, 95.40, 9.0, 2.75
1.07		1.06, 98.00, 9.6, 1.90
1.10		1.07, 99.40, 8.8, 2.15
1.155		1.08, 100.15, 9.2, 2.30
1.20	1.175, 96.1, 1.2, *	1.09, 100.60, 7.6, 2.40
1.30	1.23, 97.0, 1.7, *	1.16, 101.30, 6.5, 3.00
1.34	1.24, 97.5, 0.9, *	1.18, 101.10, 7.4, 5.50
1.40	1.285, 97.25, 2.1, 0.4	1.21, 100.90, 0.3, 3.0
1.46	1.335, 97.20, 3.3, 0.4	1.27, 100.90, 3.2, 3.0
1.51	1.370, 97.15, 3.3, 0.4	1.32, 100.50, 3.4, 3.0
1.61	1.490, 97.10, 2.8, 0.4	1.42, 100.20, 4.0, 4.0

the *HI* and *I(S)* phases. It is also tempting to speculate that this sliver of fluid connects to the IP phase shown in Fig. 2. This would suggest the IP may be a "quenched" chaotic phase.[20,21]

VI. PHASE DIAGRAM IN THE BILAYER REGION

Shown in Fig. 12 are the heat-capacity scans near 60 K of coverages above $n=1.50$. Two heat-capacity anomalies are found at 57.6 and 60.9 K, respectively. The low-temperature peak is larger and sharper than that of the high-temperature one. This double-peak structure appears at coverage near $n=1.5$ and grows until approximately $n=2.5$. Although this structure is present for all scans of higher surface coverage, the size, the location, and the shape of the anomaly do not grow with coverage above $n=2.5$.

Near the monolayer completion coverage, as we discussed in the preceding sections, 2D CF_4 solid is in the dense *HI* phase, in this phase no heat-capacity anomaly was observed in this temperature range. The appearance of this double-peak structure near $n=1.5$ is probably a sign of the formation of a bilayer solid. Our data suggest a coexistence region of the first layer and the bilayer films

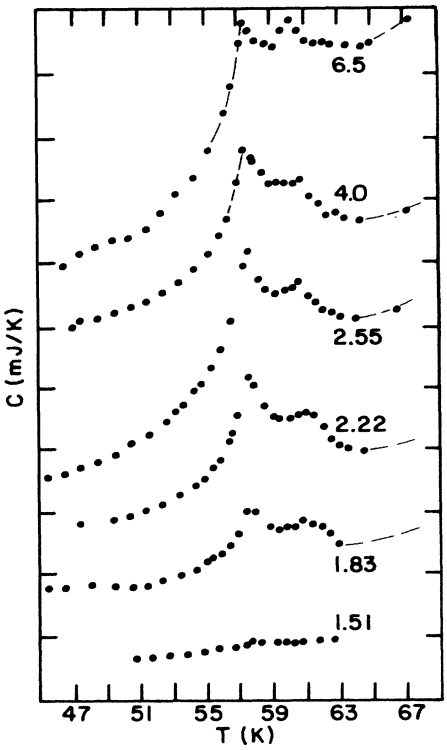

FIG. 12. Heat-capacity traces of multilayer CF_4 on graphite at temperatures near 59 K. The double-peak structures are related to transition in the bilayer system. The label on each scan is the low-temperature coverage n. The heat-capacity values at 45 K for each scan (from bottom to top) are, respectively, 1.8, 2, 2.45, 3.3, 4.3, and 8.2 mJ/K. These values correspond to approximately $8.5k_B$ per adsorbate molecule; this is somewhat larger than the expected "regular" contribution of an adsorbed film. It is possible that the transitions near 59 K extend down to 45 K.

between $n=1.5$ and 2.5 and the observed peaks are related to the phase transitions in the second layer or bilayer solid. The first monolayer completes near $n=1.5$ and bilayer completes near $n=2.5$. The fact that the bilayer completes at a coverage substantially below $n=3$ implies that during condensation of the bilayer a reconstruction of the first layer occurs. Similar behavior is seen in nitrogen on graphite during growth of the bilayer system.[25] In this reconstruction process there is a promotion of the first-layer molecules to the second layer in the bilayer solid patches. The saturation of this double-peak structure beyond $n=2.5$ indicates that no more layers form on the top of this bilayer film near 60 K. This is consistent with the picture that CF_4 does not wet graphite at low temperature.[26]

The growth of multilayer CF_4 on graphite has been studied by several experimental techniques. A vapor-pressure isotherm[2] and a neutron study[1] found that CF_4 does not wet graphite at low temperature. More recently, however, some reflection high-energy electron diffraction (RHEED) measurements[27] were interpreted as to show a first-order wetting transition of this system near 37 K. We have continued our heat-capacity study beyond the bilayar coverage and our result[26] does not show a wetting transition near 37 K. A similar conclusion is reached in an ellipsometric isotherm study.[28] The two latter experiments suggest that CF_4 does not wet graphite up to at least 80 K.[26]

Without other experimental evidence, we cannot determine the nature of the transitions for this double-peak structure. One possibility is that the peak at 57.6 K is a signature of a single layer to bilayer layering transition. This was suggested by a vapor-pressure isotherm study.[2] It is also possible that both peaks are from the bilayer film. This interpretation would suggest that the bilayer film can form on the substrate down to at least 18 K, the lowest temperature of our study. We found no evidence of any heat-capacity anomaly other than this double-peak structure below 60 K for $n>1.1$. The full size of this double-peak structure is 12 mJ. If we assume the transition involves the entire bilayer film, the entropy change associated with this anomaly is about $0.6k_B$ per molecule. This value is nearly the same as that due to the 57 K transition at submonolayer coverage from $3P$ to IP phase.

In Fig. 13, heat-capacity features near the bilayer melting temperature are presented. Between 61 and 86 K, no heat-capacity anomaly is observed within the resolution of our experiment. The small and sharp heat-capacity peak near 96 K, characteristic of the *HI* melting persists up to at least $n=2.0$. In addition to the 96-K small peak, a broad heat-capacity anomaly near 93 K, a sharp peak at 89.05 K, and a small heat-capacity signal near 86 K begin to show up near $n=1.83$ and become more prominent for scans of slightly higher ($n=2.0$) coverages. In Fig. 14, the scan at $n=1.90$ is shown with expanded heat-capacity scale. The broad peak centering at 101 K is due to the melting of the *HI* phase. The characteristics of various heat-capacity peaks in the bilayer coverage region are listed in Table IV. The effective coverage with desorption correction at each transition temperature is also shown in Table IV.

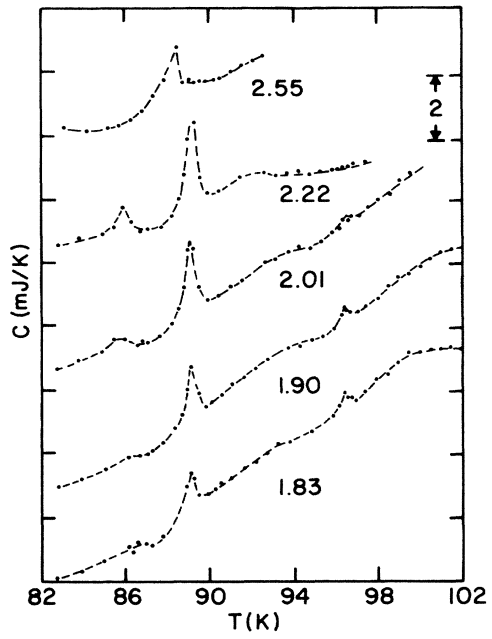

FIG. 13. Heat-capacity traces of the bilayer near the melting temperature. Heat capacity is shown in units of mJ/K. The label in each scan is the low-temperature coverage without desorption correction. For effective coverage at each transition see Table IV. The dashed lines are drawn to guide the eyes.

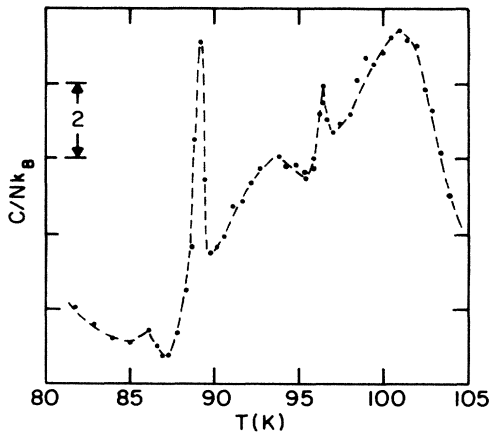

FIG. 14. Heat-capacity traces at $n=1.90$. The broad peak centering at 101 K is the transition associated with the *HI* phase melting which is truncated in Fig. 14. The data are shown in the unit of C/Nk_B, where N is the number of CF_4 molecules on the graphite surface at low temperature. For effective coverages at each transition, see Table IV.

The narrow width and the coverage range of the 89.05-K peak are evidences consistent with the interpretation that this is a signature of the melting of the bilayer system. The size of the 89.05-K peak increases with coverage from $n=1.83$ to 2.22 but the peak temperature remains constant at 89.05 K. These are signatures of coexistence and we will discuss below what are the coexisting phases. In the $n=2.55$ scan, this peak deviates from 89.05 K and shifts to 88.2 K. This indicates a change in the adsorbed film and is probably related to the completion of the bilayer.[21] When we linearly scale the peak size with coverage, we find the extrapolated coverage for zero peak size is $n=1.60$. This is the coverage where the second layer or a bilayer forms at this temperature. At low temperature the onset of the bilayer is at a coverage $n=1.5$. The difference in coverage for bilayer condensation at different temperatures can be understood in terms of an increase of the second layer gas phase with increasing temperature.

In order to understand the melting signatures of a bilayer system, we need to consider the expected behaviors for the case when the layer critical point is above and when it is below the melting temperature.

When the adsorption system is at low temperature, below the roughening temperature, first-order layer condensation occurs if surface coverage is increased isothermally. If the total coverage is between $m-1$ and m layers, there is a coexistence region of films of m layers and $m-1$ layers. With increasing temperature this coexistence region narrows and ends at a layer critical point $T_c(m)$. Above $T_c(m)$ there is no two phase coexistence region and the coverage in the adsorbed film increases with pressure continuously. This layer critical point is a reflection of the bulk roughening transition in the layered system.[8,29] In the first few layers near the substrate, depending on the relative importance of the substrate attractive field, the layer critical point can be either below or

TABLE IV. Transitions in the bilayer region near the melting temperature. For the bilayer melting peak, the four numbers represent the effective coverage, the peak position (in K), peak size (in mJ), and FWHM (in K). For the other two transitions, the two numbers are the effective coverage and the peak position. A blank space indicates the absence of the transition. It was not possible to estimate accurately the effective coverage for the $n=2.55$ scan.

n	Melting point	Critical point	*HI* phase sharp peak
1.83	1.80, 89.10, 0.7, 0.8	1.74, 93.2	1.68, 96.4
1.90	1.87, 89.10, 1.0, 0.8	1.80, 93.4	1.75, 96.4
2.01	1.97, 89.0, 1.2, 0.6	1.92, 93.0	1.87, 96.2
2.22	2.17, 89.0, 2.8, 0.6	2.13, 92.5	
2.55	88.2, 1.7, 0.8		

above the melting point of the film. If this layer critical point is below the melting temperature, the adsorbed film melts as a single-phase system (rather than one with two distinct layered films). Melting signal may still be broad compared with a true bulk system since the substrate may induce density gradient in the film. In this case the melting behavior of the adsorbed film is expected to change gradually with coverage.

If the layer critical point is above the melting temperature, the adsorbed film consists of two different phases: a film of m layers and a film of $m-1$ layers. The melting temperature for the m-layer film may be different from the $m-1$-layer film. In principle, two separate melting signals should be observed. For a bilayer film, meltings can proceed in two ways, in the first case, the top layer melts at a temperature below that of the bottom layer. This is apparently the case for O_2 on graphite.[30] It is possible that for an incomplete bilayer film, the single bottom layer and the bilayer film may melt at different temperatures. This is apparently the case for C_2H_4 on graphite.[31] Which one of the two processes will occur in a system depends on the strength of the coupling between the top and the bottom layers.

Without structural or diffraction information, we cannot unambiguously determine how the CF_4 bilayer system melts. If we assume the 89.05-K peak is due to the melting of the bilayer solid that is coexisting with a monolayer, then in the coverage range between $n=1.83$ and 2.22, the peak size divided by the number of molecules in the bilayer is a constant. This result quantitatively confirms the observation that near the melting temperature, CF_4 adlayer is in a coexistence region and melting of the bilayer occurs at a triple point. Another experimental evidence supporting this conclusion is that this 89.05-K melting signal does not evolve continuously from the first-layer melting process. In this scenario, the layer critical point is above the melting temperature of the bilayer and above 89.05 K the CF_4 system is in a coexistence region between the first layer *HI* phase and the bilayer fluid phase. This gives a reasonable and natural interpretation to the heat-capacity signal near 93 K. That is, it corresponds to crossing of the first layer *HI* solid and bilayer fluid coexistence boundary.

The discussion above follows an experimental path of constant coverage and increasing temperature. In order to see how the first-layer *HI* phase ends with increasing coverage, it may be instructive to examine the phase diagram along a path of fixed temperature and increasing coverage. Let us consider the system between 89 and 93 K starting from a coverage inside the *HI* phase ($n\sim 1.4$). With increasing coverage the system will hit the melting line (the dotted line in Fig. 2) and some of the *HI* phase melts into bilayer fluid. The size of the *HI* phase decreases with coverage until the bilayer fluid phase totally covers the substrate. This is a first-order layer condensation process. This process terminates for temperature higher than 93 K. In this sense 93 K is a bilayer critical point. Above the critical temperature, the adsorbed film does not show distinct layers. Along an isothermal path of increasing coverage from the *HI* phase at $T>93$ K, the system will melt via the weakly first-order two step process as discussed in Sec. V. In the heat-capacity scans above $n=2$, we do not observe the small, sharp peak due to the *HI* phase melting. Therefore, the *HI* phase melting line may terminate near or at the bilayer critical point. We cannot locate precisely the coverage position of this bilayer critical point. The melting transition of the *HI* phase may also smear our the bilayer critical point.

Another possibility which can explain the observed heat-capacity signals is that there is no layer critical point up to 100 K. Near the melting temperature the top layer and the bottom layer are only very weakly coupled. The

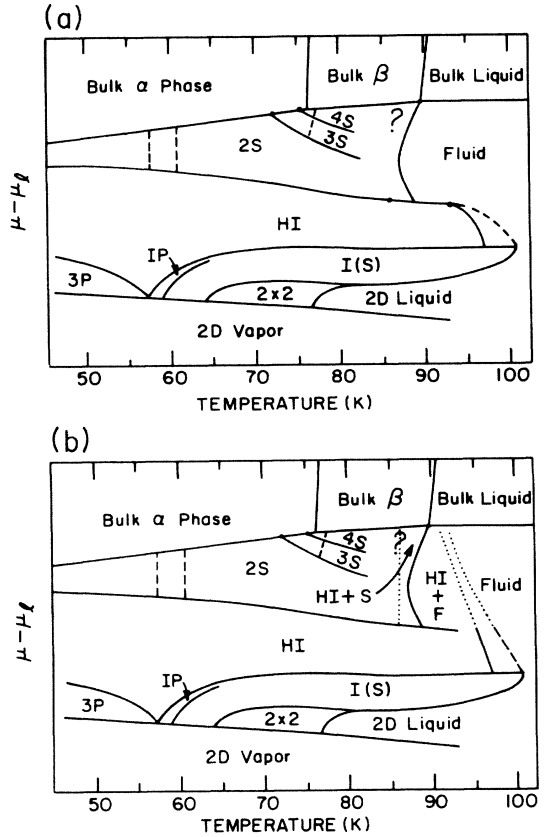

FIG. 15. Two possible phase diagrams of CF_4 on graphite in the chemical potential-temperature plane. Chemical potential is shown relative to the bulk liquid value. (a) Top panel corresponds to the situation with a bilayer critical point at 93 K. This phase diagram is consistent with Fig. 2. Dashed lines near 60 K show transitions in the bilayer film. Dashed line near 100 K is the phase boundary separating the well-correlated fluid and isotropic fluid phases. Above bilayer coverages there are layering transitions near the α-β transition (76.5 K) and a surface transition shown as a dashed line, in the nonwetting bulk clusters near 78 K, which may extend to the layered film (Ref. 27). In this case the nature of the transition at 86 K is unclear. (b) Bottom panel differs from the top one in that the *HI* phase is strongly coupled to the substrate. The transition near 86 K, therefore, can be interpreted as a decoupling process between the top layers and the first-layer *HI* phase. Above 86, K the adsorbed film consists of the bottom *HI* solid and the top solid layers. The *HI* phase melts (near 95 K) via a two step process through a well-correlated fluid region.

89.05-K melting signal is from the second layer triple point and the signal near 93 K represents the second layer liquid-vapor critical point. During these transitions, the top layer behaves like a 2D system and the bottom layer acts as an inactive substrate. In this picture, the bottom layer *HI* phase may persist up to the bulk coexistence boundary. The difficulty of this picture is that the second layer triplet point temperature seems to be too high (almost equal to the bulk triple point 89.5 K). The triple point for the monolayer as shown in Fig. 2 is at 76.3 K. Figure 2 is drawn according to the first, i.e., bilayer melting interpretation. The explanation for the heat capacity anomaly near 86 K is unclear. At $n=1.83$, 1.90, only a very weak signal shows up near 86 K. The peak position shows variation with coverage. If we use the second picture, this signal may be regarded as representing a decoupling process between the top layer and the bottom layer in the bilayer film. Corresponding to the two possibilities in the bilayer melting region, the multilayer CF_4 on graphite phase diagram in the chemical potential-temperature plane is proposed in Fig. 15. Figure 15(a) is consistent with Fig. 2, in this diagram, the bilayer coexistence line and the first layer *HI* phase melting line intersect at 93 K. The bilayer critical point may be smeared out in coverage due to the melting of the *HI* phase. Figure 15(b) is consistent with the second possibility, namely the *HI* phase behaves as a surface layer, it is strongly coupled to the substrate and persists to the multilayer region.

There are two noteworthy features in the heat-capacity behavior in the bilayer region. (1) The observed triple-point melting, although it occurs at very high temperature carries an unusual small transition heat. The size of this peak at $n=2.2$ is about 2.8 mJ. If the transition is from the bilayer film, the transition heat per CF_4 molecule is only about $10k_B$ K as compared to 42 k_B K in the first layer. (2) The phase boundary near the critical temperature at 93 K is very blunt indicating that the critical exponent β characterizing the coexistence is a very small number. This boundary resembles the 2D liquid-vapor coexistence boundary describable by the 2D Ising exponent of $\beta=\frac{1}{8}$.[32]

VII. CONCLUSIONS

In summary, we have presented a detailed phase diagram for CF_4 monolayer and bilayer adsorbed on graphite. Below monolayer completion, our data suggest a concomitant orientational ordering transition as the adsorbed solid phase transforms from $3P$ to a high-temperature incommensurate phase. This incommensurate phase, labeled as the IP phase is situated between $3P$ and $I(S)$ phases and may extend to higher coverage and temperature, e.g., sandwiched between the *HI* and $I(S)$ phases. Our data confirm the triple-point melting interpretation of the (2×2) commensurate solid at 76.3 K and we find the critical point temperature for the liquid-vapor transition at 93 ± 1 K. The very weak signal at 66.4 K for *C-I* transition is consistent with previous scattering results showing a continuous transition. We find that the melting transitions from the (2×2) and $I(S)$ phase are first order. The melting of the *HI* phase is found to be weakly first order similar to that of Ar on graphite. This result together with the Ar result suggest that the weakly first-order, two step melting may be a rather general phenomenon. Careful scattering experiments studying the well-correlated fluid may be able to determine whether this fluid is in fact the KTHNY hexatic phase.

In the bilayer coverage region, we observed the triple-point melting signature at 89.05 K and a critical point at 93 K. The layer critical point is above the melting temperature of the bilayer system. Two different possible phase diagrams in the bilayer region were proposed. We think both possibilities are physically possible and interesting. Recent heat-capacity results of C_2H_4 on graphite also found the bilayer critical point to be near 115 K, above the melting temperature of both the bilayer and monolayer.[33] These results show that near the melting temperature, the competitions between the interactions among the adsorbates and between the adsorbate and the substrate, as well as the existing thermal fluctuations can produce different paths for the monolayer phases to evolve to the multilayer region. More quantitative experimental studies in this coverage region are needed. The phase diagram in the region above the bilayer is discussed in Refs. 21 and 27. Above bilayer coverage, the melting transition temperature of the film shows variations with coverage as shown in Fig. 15. Due to desorption we cannot determine the phase diagram in the region near the bulk triple point. It is likely that a wetting transition may occur near the bulk triple point that changes the CF_4 on graphite system from nonwetting to wetting growth.

ACKNOWLEDGMENTS

We wish to thank P. Dutta and S. K. Sinha for useful conversations. This work was supported by the NSF through Grant Nos. DMR-8419261 and DMR-8206109 (low-temperature physics).

*Present address: Department of Physics, Pusan National University, Pusan, Korea.

[1]B. Croset, C. Marti, P. Thorel, and H. Lauter, J. Phys. (Paris) **43**, 1659 (1982); H. J. Lauter, B. Croset, C. Marti, and P. Thorel, in *Ordering in Two Dimensions*, edited by S. K. Sinha (North-Holland, New York, 1980).

[2]P. Dolle, M. Matecki, and A. Thomy, Surf. Sci. **91**, 271 (1980).

[3]P. S. Calisti, Ph.D. thesis, University of Marseille, 1981.

[4]K. Kjaer, M. Nielsen, J. Bohr, H. J. Lauter, and J. P. McTague, Phys. Rev. B **26**, 5168 (1982); Surf. Sci. **125**, 171 (1983).

[5]S. E. Nagler, P. Dutta, P. M. Horn, S. K. Sinha, and D. E. Moncton, Bull. Am. Phys. Soc. **30**, 334 (1985); and private communications from P. Dutta and S. K. Sinha.

[6]P. Bak and T. Bohr, Phys. Rev. B **27**, 591 (1983).

[7]M. Schick, Surf. Sci. **125**, 94 (1983).

[8]R. Pandit, M. Schick, and M. Wortis, Phys. Rev. B **26**, 5112 (1982).

[9]P. W. Stephens, P. A. Heiney, R. J. Birgeneau, P. M. Horn, D. E. Moncton, and G. S. Brown, Phys. Rev. B **29**, 3512 (1984); E. D. Specht, M. Sutton, R. J. Birgeneau, D. E. Moncton, and P. M. Horton, *ibid.* **30**, 1589 (1984); K. L. D'Amico, D. E. Moncton, E. D. Specht, R. J. Birgeneau, S. E. Nagler, and P. M. Horn, Phys. Rev. Lett. **53**, 2250 (1984).

[10]Q. M. Zhang, H. K. Kim, and M. H. W. Chan, Phys. Rev. B **32**, 1820 (1985).

[11]M. H. W. Chan, A. D. Migone, K. D. Miner, and Z. R. Li, Phys. Rev. B **30**, 2681 (1984).

[12]A. D. Migone, Z. R. Li, and M. H. W. Chan, Phys. Rev. Lett. **53**, 810 (1984).

[13]Q. M. Zhang, H. K. Kim, and M. H. W. Chan, Phys. Rev. B **33**, 5149 (1986).

[14]H. Enokido, T. Shinoda, and Yo-Ichiro Mashiko, Bull. Chem. Soc. Jpn. **42**, 3415 (1969); J. H. Smith and E. L. Pace, J. Phys. Chem. **73**, 4232 (1969).

[15]A. D. Migone, M. H. W. Chan, K. J. Niskanen, and R. B. Griffiths, J. Phys. C **16**, L1115 (1983); D. M. Butler, J. A. Litzinger, G. A. Stewart, and R. B. Griffiths, Phys. Rev. Lett. **42**, 1289 (1979).

[16]K. J. Niskanen and R. B. Griffiths, Phys. Rev. B **32**, 5868 (1985); K. J. Niskanen, *ibid.* **33**, 1830 (1986).

[17]Kr on graphite at submonolayer, T_t(2D) is 84.8K; T_t(3D), 115.76 K; T_c(3D), 209.4 K; N_2, T_t(2D), 49 K; T_t(3D), 63.17; T_c(3D), 126.2 K.

[18]H. K. Kim, Q. M. Zhang, and M. H. W. Chan, J. Chem. Soc., Faraday Trans. II (1986); see comments by M. E. Fisher and M. H. W. Chan at the end of this paper.

[19]S. K. Ma, *Modern Theory of Critical Phenomena* (Benjamin-Cummings, Menlo Park, California, 1976).

[20]S. N. Coppersmith, D. S. Fisher, B. I. Halperin, P. A. Lee, and W. F. Brickman, Phys. Rev. Lett. **46**, 549 (1982); Phys. Rev. B **25**, 349 (1982); M. Kardar and A. N. Berker, Phys. Rev. Lett. **48**, 1552 (1982); R. G. Caflisch, A. N. Berker and M. Kardar, Phys. Rev. B **31**, 4527 (1985); D. A. Huse and M. E. Fisher, Phys. Rev. Lett. **49**, 793 (1982); Phys. Rev. B **29**, 229 (1984); Per Bak, Rep. Prog. Phys. **45**, 587 (1982).

[21]Q. M. Zhang, Ph.D. thesis, The Pennsylvania State University, 1986.

[22]J. M. Kosterlitz and D. J. Thouless, J. Phys. C **6**, 1181 (1973); D. R. Nelson and B. I. Halperin, Phys. Rev. B **19**, 2457 (1979); A. P. Young, Phys. Rev. B **19**, 1855 (1979).

[23]Y. Saito, Phys. Rev. Lett. **48**, 1114 (1982); Phys. Rev. B **26**, 6239 (1982).

[24]S. T. Chui, Phys. Rev. Lett. **48**, 933 (1982); Phys. Rev. B **28**, 178 (1983).

[25]Q. M. Zhang, H. K. Kim, and M. H. W. Chan, Phys. Rev. B **33**, 413 (1986).

[26]Q. M. Zhang, H. K. Kim, and M. H. W. Chan, Phys. Rev. B **34**, 2056 (1986).

[27]J. Suzanne, J. L. Seguin, M. Bienfait, and E. Lerner, Phys. Rev. Lett. **52**, 637 (1984); J. M. Gay, M. Bienfait, and J. Suzanne, J. Phys. (Paris) **45**, 1497 (1984).

[28]M. Drir, H. J. Nham, and G. B. Hess, Bull. Am. Phys. Soc. **30**, 412 (1985); and unpublished.

[29]M. J. de Oliveria and R. B. Griffiths, Surf. Sci. **71**, 687 (1978).

[30]S. Mochrie, M. Sutton, J. Akimitsu, R. J. Birgeneau, P. M. Horn, P. Dimon, and D. Moncton, Surf. Sci. **138**, 599 (1984).

[31]S. Mochrie, M. Sutton, R. J. Birgeneau, D. E. Moncton, and P. M. Horn, Phys. Rev. B **30**, 263 (1984); H. K. Kim, Q. M. Zhang, Y. P. Feng, and M. H. W. Chan (unpublished).

[32]H. K. Kim and M. H. W. Chan, Phys. Rev. Lett. **53**, 170 (1984).

[33]Q. M. Zhang, Y. P. Feng, H. K. Kim, and M. H. W. Chan, Phys. Rev. Lett. **57**, 1456 (1986).